Dielectrophoretic Manipulation of Particles and Cells Using Insulating Ridges in Faceted Prism Microchannels

Louise M. Barrett,* Andrew J. Skulan, Anup K. Singh, Eric B. Cummings, and Gregory J. Fiechtner

Sandia National Laboratories, Livermore, California 94551

This paper presents a novel device for the dielectrophoretic manipulation of particles and cells. A two-level isotropic etch of a glass substrate was used to create three-dimensional ridge-like structures in micrometer-sized channels. Due to the insulating properties of glass, locally patterned regions of nonuniform electric field form near the ridges when a dc field is applied along the channel. The ridges are designed using the method of faceted prisms, such that substantially uniform fields are produced on each side of the faceted interfaces that form each ridge. The dielectrophoretic force that results from the electric field gradient near the ridges is used to affect particle motion parallel to the ridges in the absence of a bulk pressure-driven flow. Trapping and deflection of particles and continuous concentration and separation of *Bacillus subtilis* from a two-component sample mixture are demonstrated. The flow of *B. subtilis* is restricted to a selected channel of a planar, multichannel device as a result of negative dielectrophoresis arising from the presence of the insulating ridges when the applied electric field exceeds a threshold of 30 V/mm. Dielectrophoresis has a negligible impact on 200-nm-diameter polystyrene particles under the same conditions.

New and improved techniques to characterize and sort microscopic-sized particles and cells are in high demand for a wide range of applications in areas such as biomedical research, clinical diagnostics, and environmental analysis. During sample preparation, trapping of particles facilitates automation of labor-intensive procedures such as filtration, washing, and labeling. During sample analysis, the ability to direct particles selectively down a specific channel to an appropriate assay is useful. Also, during analysis, trapping of particles in specific regions of a chip concentrates the particles, potentially enhancing reaction times, reducing reagent volumes, and improving detection limits. Having the ability to support both sample preparation and analysis, dielectrophoresis (DEP)[1] is an effective way to trap, manipulate, and separate a variety of particles such as ores,[2] clays,[3] bacteria,[4,5]

yeast cells,[6,7] large DNA strands,[8] mammalian cells,[9,10] blood cells,[10–12] cancer cells,[12–16] malaria-infected blood cells,[17–19] CD 34 stem cells,[20,21] viruses,[22–24] and latex particles.[25–27]

DEP is the movement of polarizable and conductive particles toward or away from regions of high electric field intensity in nonuniform electric fields.[27] When particles approach a field gradient, they experience a selective force owing to DEP that is proportional to the particle volume and the difference in complex conductivity of the particle and the fluid.[28] Depending on the relative magnitude of the particle conductivity and that of the fluid, the DEP force can act to drive particles toward regions of either high electric field strength or low electric field strength—types

* To whom correspondence should be addressed. E-mail: lmbarre@sandia.gov.

(1) Gascoyne, P. R. C.; Vykoukal, J. *Electrophoresis* **2002**, *23*, 1973−1983.
(2) Lin, I. J.; Benguigui, L. *Sep. Purif. Methods* **1981**, *10*, 53−72.
(3) Lockhart, N. C. *Powder Technol.* **1983**, *35*, 17−22.
(4) Wang, X.-B.; Huang, Y.; Burt, J. P. H.; Markx, G. H.; Pethig, R. *J. Phys. D* **1993**, *26*, 1278−1285.
(5) Allsopp, D. W. E.; Milner, K. R.; Brown, A. P.; Betts, W. B. *J. Phys. D: Appl. Phys.* **1999**, *32*, 1066−1074.
(6) Pethig, R.; Huang, Y.; Wang, X.-B.; Burt, J. P. H. *J. Phys. D* **1992**, *25*, 881−888.
(7) Markx, G. H.; Talary, M. S.; Pethig, R. *J. Biotechnol.* **1994**, *32*, 29−37.
(8) Asbury, C. L.; Diercks, A. H.; Van den Engh, G. *Electrophoresis* **2002**, *23*, 2658−2666.
(9) Gascoyne, P. R. C.; Huang, Y.; Pethig, R.; Vykoukal, J.; Becker, F. F. *Meas. Sci. Technol.* **1992**, *3*, 439−445.
(10) Xu, C. X.; Wang, Y.; Cao, M.; Lu, Z. H. *Electrophoresis* **1999**, *20*, 1829−1831.
(11) Auerswald, J.; Knapp, H. F. *Microelectron. Eng.* **2003**, *67−68*, 879−886.
(12) Becker, F. F.; Wang, X.-B.; Huang, Y.; Pethig, R.; Vykoukal, J.; Gascoyne, P. R. C. *J. Phys. D* **1994**, *27*, 2659−2662.
(13) Becker, F. F.; Wang, X.-B.; Huang, Y.; Pethig, R.; Vykoukal, J.; Gascoyne, P. R. C. *Proc. Natl. Acad. Sci. U.S.A.* **1995**, *92*, 860−864.
(14) Gascoyne, P. R. C.; Wang, X. B.; Huang, Y.; Becker, F. F. *IEEE Trans. Ind. Appl.* **1997**, *33*, 670−678.
(15) Cheng, J.; Sheldon, E. L.; Wu, L.; Heller, M. J.; O'Connell, J. P. *Anal. Chem.* **1998**, *70*, 2321−2326.
(16) Burt, J. P. H.; Pethig, R.; Gascoyne, P. R. C.; Becker, F. F. *Biochim. Biophys. Acta* **1990**, *1034*, 93−101.
(17) Gascoyne, P.; Pethig, R.; Satayavivad, J.; Becker, F. F.; Ruchirawat, M. *Biochim. Biophys. Acta* **1997**, *1323*, 240−252.
(18) Gascoyne, P.; Mahidol, C.; Ruchirawat, M.; Satayavivad, J.; Watcharasit, P.; Becker, F. F. *Lab Chip* **2002**, *2*, 70−75.
(19) Gascoyne, P.; Satayavivad, J.; Ruchirawat, M. *Acta Trop.* **2004**, *89*, 357−369.
(20) Stephens, M.; Talary, M. S.; Pethig, R.; Burnett, A. K.; Mills, K. I. *Bone Marrow Transplant.* **1996**, *18*, 777−782.
(21) Talary, M. S.; Mills, K. I.; Hoy, T.; Burnett, A. K.; Pethig, R. *Med. Biol. Eng. Comput.* **1995**, *33*, 235−237.
(22) Green, N. G.; Morgan, H.; Milner, J. J. *J. Biochem. Biophys. Methods* **1997**, *35*, 89−102.
(23) Morgan, H.; Green, N. G. *J. Electrost.* **1997**, *42*, 279−293.
(24) Muller, T.; Fiedler, S.; Schnelle, T.; Ludwig, K.; Jung, H.; Fuhr, G. *Biotechnol. Tech.* **1996**, *10*, 221−226.
(25) Green, N. G.; Morgan, H. *J. Phys. D* **1997**, *30*, 2626−2633.
(26) Green, N. G.; Morgan, H. *J. Phys. D* **1997**, *30*, L41−L44.
(27) Pohl, H. A. *Dielectrophoresis*; Cambridge University Press: Cambridge, 1978.
(28) Benguigui, L.; Lin, I. J. *J. Phys. D* **1984**, *17*, L9−L12.

of DEP termed positive and negative, respectively. The DEP force can be used to trap, deflect, and manipulate cells and particles.

Most commonly, DEP is driven by electric field nonuniformities arising from multiple electrodes embedded throughout a fluidic system. Recently, insulator-based dielectrophoresis (IDEP) has shown great promise as an alternative approach to conventional DEP. In IDEP, insulating structures (i.e., packing material,[29-34] posts, or ridges[35-38]) result in gradients in local electric field, which is imparted using electrodes located only at the channel inlet and channel outlet. If the applied field has a dc component, this field can also produce an electrokinetic flow through the channel. In early realizations of IDEP, then called "multigradient DEP",[39,40] the space between electrodes was packed with insulating material such as glass beads[29,30,33,34] and particles were dielectrophoretically trapped in regions between the beads. While the resulting early devices were simple to construct and operate, design methods were not employed to pattern local field gradients. The advent of planar micromanufacturing has enabled the rational design of insulating structures for IDEP, and more recently, a single, isotropic etch was used to fabricate insulating structures in precise arrays of a chosen geometric design.[41-43] Here, the requisite field gradients for DEP result from such insulating structures, and therefore, the technique has been called "insulator-based"[36,37] or "electrodeless"[35,41] DEP. Transport in microchannels containing arrays of insulating obstacles has been modeled using a Laplace solver based on the theory of ideal electrokinetic flow.[42] Experimental demonstrations of system designs arising from such modeling included localized arrays of particle-trapping structures, rows of concentrated particle streams, or both.[36,37,43] Selective concentration of particles, including polystyrene latex spheres,[42] bacteria,[36,37] and DNA[35] has been shown using IDEP. Moreover, selective local concentration has been produced between combinations of samples, including species of bacteria,[36] bacteria and latex polystyrene beads,[37] and viable and nonviable organisms.[37]

We report on an important extension of the IDEP technique in which generation of uniform field gradients spanning an entire channel width is achieved through the use of microfluidic channels having two distinct channel depths.[44-46] This work takes advantage of the flexibility afforded by a dual-depth glass-etching technique to construct insulating ridges along which particles are deflected, trapped, or both. For a ridge to function as a selective filter/concentrator, it is desirable to have spatially uniform fields on both sides of the interface (the leading edge of the ridge) between deep and shallow regions. The result is a field gradient that is uniform along a line parallel to the interface. Consequently, the ridge deflects particles uniformly along its entire leading (or trailing) edge. Without a channel design that produces uniform fields on each side of the ridge, DEP-induced particle motion will also vary along the ridge, allowing particles that are deflected or trapped at one side of the microchannel to pass over the ridge unaffected at other locations within the microchannel. To this end, we employ faceted prisms to fabricate insulating ridges.[47,48] The technique was introduced by Fiechtner and Cummings,[47] who derived the design rules theoretically that are necessary for the design of ideal prismatic sections. In a companion paper,[49] we present the first experimental demonstration of faceted prism microchannels, in which fields are applied at low levels, and images of the resulting velocity fields are obtained using particle image velocimetry. In the present paper, we present the first demonstration of the faceted prism methodology for particle filtration and concentration by dielectrophoresis at comparatively large applied fields. The resulting insulating ridges are fabricated in a glass microfluidic device in which carboxylate-modified polystyrene particles are trapped and concentrated experimentally. Finally, a two-component mixture of particles and vegetative *Bacillus subtilis* are fractionated, demonstrating the ability of the IDEP system to concentrate bacteria quickly and selectively.

EXPERIMENTAL SECTION

Chip Fabrication. The microfluidic chips were fabricated from D263 glass substrates (100-mm diameter, 1.1mm thick, S. I. Howard Glass Co., Worcester, MA) using standard photolithography, wet etch, and bonding techniques. To fabricate the ridge structures, a two-step etch process was employed.[44-46] After completion of the initial etch step, the etch process was repeated using a different mask, resulting in trenches having regions of two distinct depths. The mask for the second etch was aligned with the first etch through the use of a pair of alignment marks located near the outer edges of the wafer. The alignment marks on the mask were overlaid with those on the wafer using a MA-6 Karl Suss aligner. Lids were formed using the same glass material (D263 glass) as the etched substrate. Via access holes were drilled in the cover plate with diamond-tipped drill bits (Amplex, Worcester, MA). The etched wafer and drilled cover plate was cleaned with 4:1 H_2SO_4/H_2O_2 (100 °C). The machined cover plate was rinsed with 1% HF solution to inhibit crack propagation. The substrates were then immersed in a 40% NaOH solution at 80 °C, rinsed in a cascade bath, spun dry, aligned for contact, and thermally bonded by slowly ramping the temperature to 610 °C for 5 h in a nitrogen-purged programmable muffle furnace (model 48000, Thermolyne Dubuque, IA).

(29) Benguigui, L.; Lin, I. J. *J. Appl. Phys.* **1984**, *56*, 3294−3297.
(30) Lin, I. J.; Benguigui, L. *J. Electrost.* **1982**, *13*, 257−278.
(31) Lin, I. J.; Benguigui, L. *Sep. Sci. Technol.* **1982**, *17* (5), 645−654.
(32) Suehiro, J.; Zhou, G. B.; Imamura, M.; Hara, M. *IEEE Trans. Ind. Appl.* **2003**, *39*, 1514−1521.
(33) Benguigui, L.; Lin, I. J. *Sep. Sci. Technol.* **1982**, *17*, 1003−1017.
(34) Zhou, G.; Imamura, M.; Suehiro, J.; Hara, M., 37th Annual Meeting of the IEEE-Industry-Applications-Society, Pittsburgh, PA, *Proc. IEEE* **2002**; pp 1404−1411.
(35) Chou, C.-F.; Tegenfeldt, J. O.; Bakajin, O.; Chan, S. S.; Cox, E. C.; Darnton, N.; Duke, T.; Austin, R. H. *Biophys. J.* **2002**, *83*, 2170−2179.
(36) Lapizco-Encinas, B. H.; Simmons, B. A.; Cummings, E. B.; Fintschenko, Y. *Electrophoresis* **2004**, *25*, 1695−1704.
(37) Lapizco-Encinas, B. H.; Simmons, B. A.; Cummings, E. B.; Fintschenko, Y. *Anal. Chem.* **2004**, *76*, 1571−1579.
(38) Xuan, X. C.; Xu, B.; Li, D. Q. *Anal. Chem.* **2005**, *77*, 4323−4328.
(39) Shalom, A. L.; Lin, I. J. *Sep. Purif. Methods* **1987**, *16*, 1−30.
(40) Shalom, A. L.; Lancelot, F.; Lin, I. J. *Sep. Sci. Technol.* **1989**, *24*, 179−197.
(41) Chou, C.-F.; Zenhausern, F. *IEEE Eng. Med. Biol. Mag.* **2003**, *22*, 62−67.
(42) Cummings, E. B.; Singh, A. K. *Anal. Chem.* **2003**, *75*, 4724−4731.
(43) Cummings, E. B. *IEEE Eng. Med. Biol. Mag.* **2003**, *22*, 75−84.
(44) Kirby, B. J.; Reichmuth, D. S.; Renzi, R. F.; Shepodd, T. J.; Wiedenman, B. J. *Lab Chip* **2005**, *5*, 184−190.
(45) Reichmuth, D. S.; Shepodd, T. J.; Kirby, B. J. *Anal. Chem.* **2004**, *76*, 5063−5068.

(46) Fruetel, J. A.; Renzi, R. F.; VanderNoot, V. A.; Stamps, J.; West, J. A. A.; Ferko, S.; Crocker, R.; Bailey, C. G.; Arnold, D.; Wiedenman, B.; Choi, W.-Y.; Yee, D.; Shokair, I.; Hasselbrink, E.; Paul, P.; Rakestraw, D.; Padgen, D. *Electrophoresis* **2005**, *26*, 1144−1154.
(47) Fiechtner, G. J.; Cummings, E. B. *Anal. Chem.* **2003**, *75*, 4747−4755.
(48) Fiechtner, G. J.; Cummings, E. B. *J. Chromatogr., A* **2004**, *1027*, 245−257.
(49) Skulan, A. J.; Barrett, L. M.; Singh, A. K.; Cummings, E. B.; Fiechtner, G. J. *Anal. Chem.* **2005**, *77*, 6790−6797.ac050777g

Cell Preparation. *B. subtilis* (strain ATCC #6633) was obtained from ATCC (Manassas, VA) and grown in Luria-Bertani (LB) nutrient broth. Cultures were grown overnight at 37 °C in an incubator to achieve saturation conditions. A 1:10 volumetric dilution of the cell culture was then allowed to grow in the LB liquid broth into late log phase to a cell concentration of 6×10^8 cells/mL, verified by OD measurements at 600 nm.[50] Cells were centrifuged at 5000 rpm for 120 min to eliminate the LB nutrient broth. The cells were resuspended in deionized (DI) water using a vortex mixer. The cells were then labeled with Syto11 (green) or Syto17 (red) (Molecular Probes, Inc., Eugene, OR). For every milliliter of cell culture present in the vial containing the live cells, 3 μL of the Syto dye was added. The cells were then incubated at room temperature for 10 min, concentrated by centrifugation at 5000 rpm for 10 min, washed with DI water to remove any free dye, and resuspended in DI water to the desired final volume to reach the appropriate cell concentration (typically 6×10^8 cells/mL). The DI water employed had a conductivity of 10 μS/mm, pH 7.7 (adjusted using concentrated sodium hydroxide) (Millipore).

DEP Experiments. Pipet tips were used as fluid reservoirs and care was taken to minimize pressure-driven flow produced by liquid-level differences in the reservoirs before each run. A sample of labeled cells, inert carboxylate-modified polystyrene particles (Fluospheres, Molecular Probes, Eugene OR), hereafter referred to as 200-nm particles, or a mixture of both, were introduced at the inlet reservoir and outlet reservoir. Here the channels of the devices were filled with particles in the absence of an applied field. Some particles can get lodged on the ridges during this filling stage—unwanted particle adhesion is often observed, becoming increasingly prevalent as a chip is reused from day-to-day. *B. subtilis* can be washed from channels between experimental runs using surfactants, but this approach is less effective for the removal of polystyrene particles. Therefore, to minimize the influence of lodged particles, data were collected using chips that were reused only a few times. Electrodes were placed at the inlet and outlet reservoirs and an electric field was applied along the microchannel. The distance between the two electrodes was 10.2 mm. A high-voltage power supply (Stanford Research Systems, PS350, Palo Alto, CA) was used to apply electric fields by employing platinum wire electrodes with a 0.5-mm diameter (Omega Engineering Inc., Stamford, CT). Therefore, the reported field strengths (V/mm) represent nominal electric field strength, with the voltage applied along the entire 10.2-mm distance between electrodes. The behavior of the cells and inert particles was imaged using an inverted epifluorescence microscope (model IX-70, Olympus, Melville, NY) equipped with filter sets for dual-color imaging of red and green dyes (51006, Chroma Technologies Corp, Brattleboro, VT) and single-color imaging of green dye (Olympus U-MNB, Olympus, Melville, NY). Images were captured using a digital camera (Sony, San Diego, CA) and an image acquisition program (written in-house).

DEP Simulations. Simulations of the electrokinetic flow were performed using a previously reported electrokinetic and dielectrophoretic simulation code.[42] These qualitative simulations elucidate how particles will behave in a device with regions of
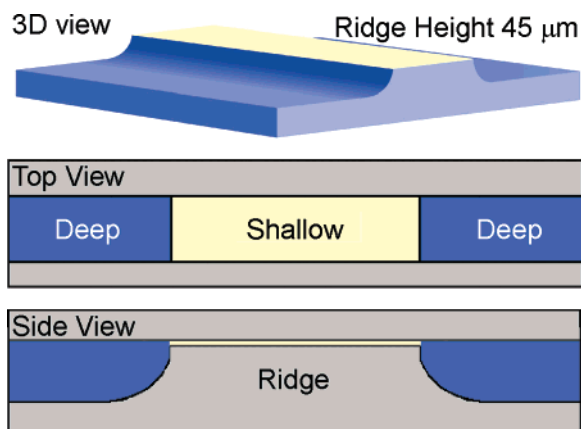
(50) Ausubel, F. M.; Brent, R.; Kingston, R. E.; Moore, D. D.; Seidman, J. G.; Smith, J. A.; Struhl, K. *Short Protocols in molecular Biology*, 5th ed.; Wiley: New York, 2002.

Figure 1. Schematic representations of an insulative ridge created using a two-level isotropic etch of glass. The deep region (blue) is 50 μm deep, and the shallow region (yellow) is 5 μm deep.

nonuniform field strengths under conditions where DEP is negligible and those where DEP is significant. For illustration purposes, all the simulation diagrams follow a narrow band of particles and their relative positions at a certain point in time (tX). The numerical simulation approach solves the modified Laplace equation, $\sigma(x,y)\nabla\varphi(x,y) = 0$ for the electrostatic potential φ at each point in a two-dimensional field σ that is proportional to the depth of the channel. The electrokinetic velocity of a particle is given by $u_{EK} = \mu_{EK}E$, where μ_{EK} is the electrokinetic mobility of the particle and E is the local electric field ($E = -\varphi(x,y)$). The dielectrophoretic velocity is $u_{DEP} = \mu_{DEP}\nabla(E \cdot E)$, where μ_{DEP} is the dielectrophoretic mobility of the particle. Expressing the electrokinetic velocity as $\mu_{EK} \equiv \mu_{EP} - \mu_{EO}$, where μ_{EO} and μ_{EP} are the electroosmotic and electrophoretic mobilities, respectively, we obtain the expression describing that, for deflection or trapping to occur,[36]

$$\frac{u_{DEP} \cdot u_{EK}}{u_{EK} \cdot u_{EK}} = \frac{\mu_{DEP}}{(\mu_{EP} - \mu_{EO})} \frac{\nabla l}{l} \cdot E > 1 \qquad (1)$$

where $l \equiv E \cdot E$ is the local field intensity.

At low field strengths, the electrokinetic force component dominates, while at high field strengths, the dielectrophoretic force component dominates in regions having local field gradients, such as at the interface between deep and shallow depth regions of a channel. For simplicity and clarity, the analysis presented here treats particles as infinitesimal points that are in local electrostatic equilibrium. The simulations neglect motion resulting explicitly from hydrodynamic lift and drag, buoyancy, finite polarization rate, and finite particle size effects.

RESULTS AND DISCUSSION

A schematic representation of the insulating ridge geometry used in this work is shown in Figure 1. Simulation results for a straight channel with a ridge oriented perpendicular to the flow direction are shown in Figure 2.[49] This type of ridge represents the most trivial form of faceted prism, taken from a larger family of uniform-field designs.[47,48] The simulation was performed under conditions for which DEP is negligible (Figure 2a) and also when DEP is significant (Figure 2b). As can be observed in the
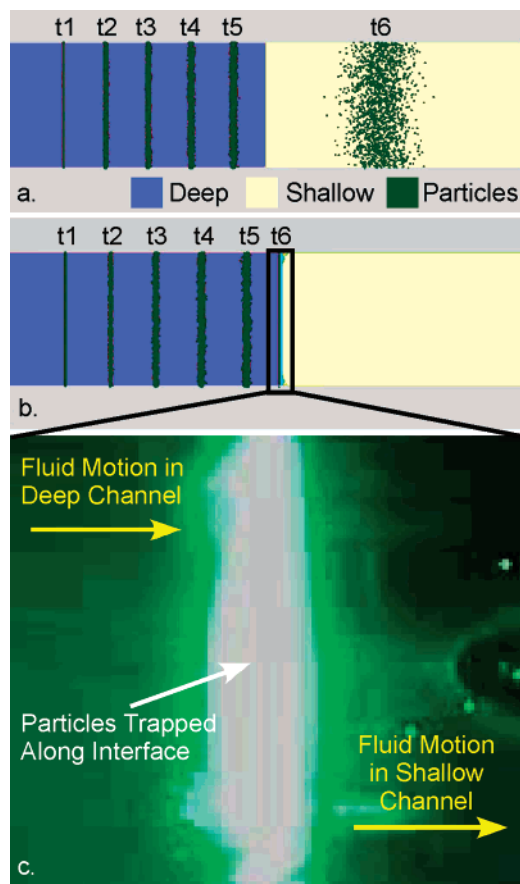
Figure 2. Particle trapping at a ridge. (a) Simulation below DEP inhibition threshold, particles flow over the ridge. (b) Simulation above DEP inhibition threshold, particles trap just before the ridge. The deep region (blue) is 50 μm deep, and the shallow region (yellow) is 5 μm deep. (c) Fluorescence image showing trapping of 200-nm particles at a ridge with an applied field strength of 100 V/mm.

Figure 3. Vector diagram of the forces proportional to that caused by electrokinetic and dielectrophoretic effects, $\mathbf{F}_{EK}$ and $\mathbf{F}_{DEP}$, respectively, for a particle near a faceted-prism interface. For nonzero interface angles, θ, the particle acquires a net motion parallel to the vector $\mathbf{F}_{NET}$.

2. Here, the particles trap near the interface, where electrokinetic and dielectrophoretic forces balance. Alternatively, a faceted interface oriented at a nonzero angle θ with respect to the direction of flow allows the possibility of net motion, as is illustrated in the vector diagram of Figure 3. Here, the field gradient, and hence, the direction that dielectrophoresis pushes the particles, no longer aligns with the incident electrokinetic field. The result is that particles are deflected along the ridge. This can be used, for example, to trap particles at a point (in contrast to trapping along a line, as is demonstrated in Figure 2).

Alternatively, angled interfaces can be used to deflect particles continuously to a separate "concentration" channel. The faceted prism methodology can be used to design a variety of microchannels, including flow splitters that divide an inlet channel into any number of outlet channels. Motivated by such faceted flow-splitter designs,[48] a three-way flow splitter was designed and fabricated using the faceted prism geometry shown in Figure 4. Here, a single, 50-μm-deep inlet is split into three 50-μm-deep outlets. Two of the side channels have angled, faceted prism ridges (45 μm high) at their entrances, while the center channel contains no faceted prism ridge. Figure 4c and 4d show simulation results for a single-particle type migrating through the pitchfork geometry at applied field strengths below (c) and above (d) the inhibition threshold. In this case, the simulation includes effects such as etch-back that cause deviation from exact mathematical designs.[49] To demonstrate particle motion, bands of particles are superimposed on the flow inlet at time t1, and tracked through the channel for later instances t2−t5. As shown, particles flow exclusively out of the central channel when fields above the inhibition threshold are applied. For the present channel depths, the isotropic etching technique of channel fabrication causes deviations of channel geometry from ideal theory. Moreover, placement of the central channel also causes additional deviation from ideal designs. Nevertheless, the simulations show that, above some threshold, particle deflection to the central channel should occur. Figure 5 shows the cross-facet values of E (black line) and $\nabla(E \cdot E)$ (red line), proportional to the electrokinetic and dielectrophoretic forces, $\mathbf{F}_{DEP}$ and $\mathbf{F}_{EK}$, respectively, exerted on a particle. For DEP trapping or deflection to occur, $\mathbf{F}_{DEP}$ has to be greater than $\mathbf{F}_{EK}$ such that the conditions of eq 1 are satisfied.[36, 42]

The simulations of Figure 4 identify significant band dispersion and bending in the central concentration channel. The amount of

simulation results, when DEP is insignificant (at low applied electric fields), the particles flow unhindered over the ridge.[49] Above a threshold applied electric field, which depends, in part, on the particle physical properties, DEP becomes appreciable and particles entering the system are inhibited from crossing the interface. Here, the value of this "inhibition threshold" depends on the ratio of the electrokinetic and dielectrophoretic particle mobility as governed by eq 1,[42] and the specific permeability ratio of the faceted prism ridge, where, for example, an increase of the specific permeability ratio results in a larger field gradient between deep and shallow sections, such that $\mu_{DEP}\nabla(E\cdot E)$ is correspondingly increased. The threshold value was examined experimentally for 200-nm particles, and the results are shown in Figure 2c. Here, it is observed that when DEP is significant—in this case for an applied field strength of 100 V/mm or larger—trapping occurs along the leading interface of the ridge. A device such as this is useful for filtering or concentrating one type of particle from a sample of particles. Washing steps or labeling could be performed while the particles are trapped.

The device function is inherently altered by changing the incidence angle of the faceted prism (known as the interface angle for the ridge[47,48]). This is illustrated by the vector diagrams of Figure 3. The case for which $\theta = 0$ corresponds to a facet oriented perpendicular to the direction of flow, as was considered in Figure
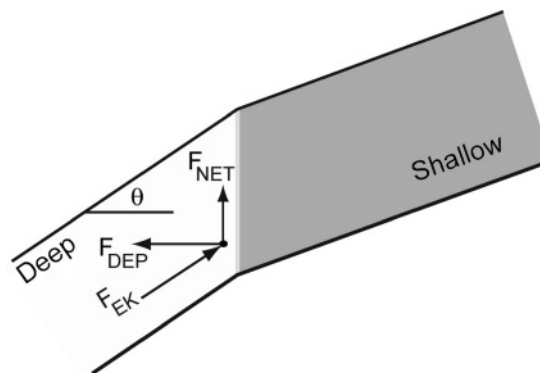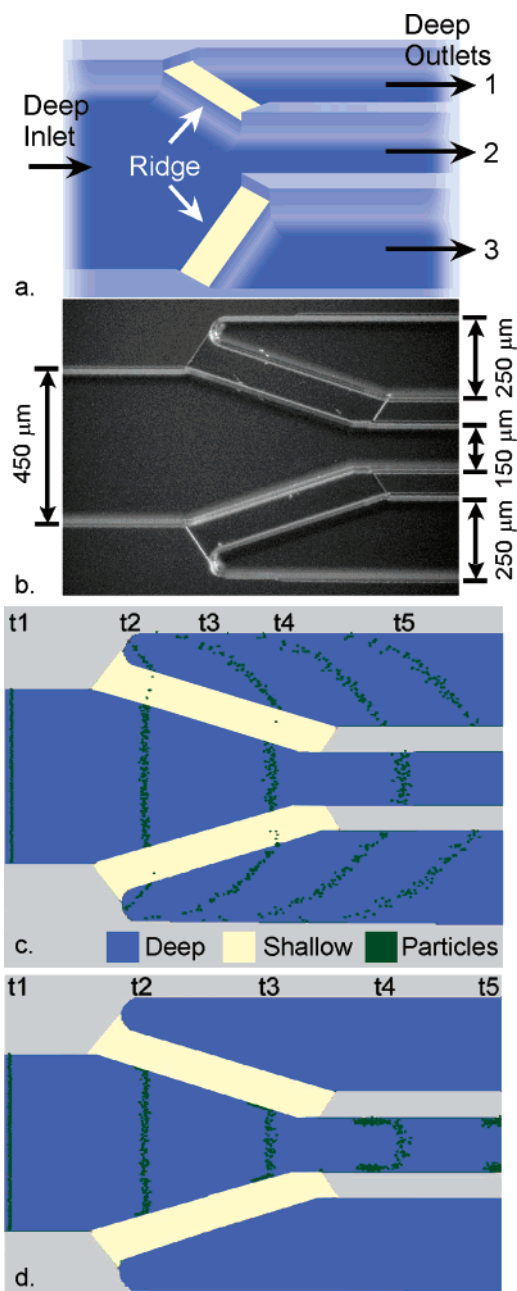
Figure 4. Planar glass pitchfork channel geometry. (a) Schematic representation of two ridges in a channel with one inlet (left) and three outlets (right). (b) Micrograph of manufactured device. Length from inlet to outlet ports was 10.2 mm. (c) Simulation below DEP threshold, particles flow over the insulative ridges and out through the three channels. (d) Simulation above DEP threshold, particles are deflected by the insulative ridge and confined to the central channel. The deep region (blue) is 50 μm deep, and the shallow region (yellow) is 5 μm deep. Flow is from left to right.

dispersion is larger when DEP is dominant (Figure 4d, t4) than for the low-field example of Figure 4c. The larger dispersion when DEP is significant results from the deflection transit and delay that results for particles in the vicinity of an interface. If a sample was injected in a short window, as signified by line t1 in Figure 4d, then the resulting sample band that would arrive in the concentration channel at time t5 would be broadened by dispersion. This broader sample peak would require a wider temporal window when detecting with downstream analytical instruments.
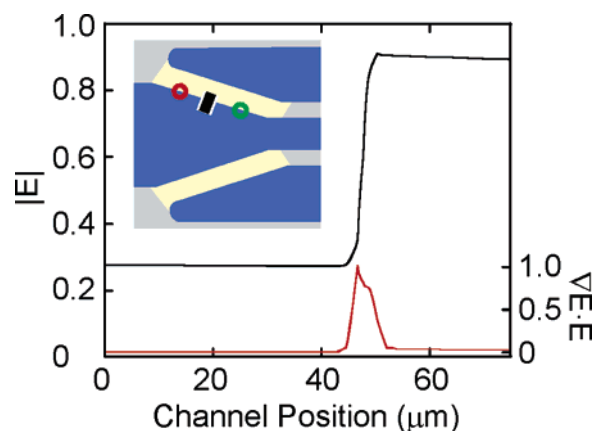
Figure 5. Cross-facet electrokinetic (|E|, black line) and dielectrophoretic ($\nabla E \cdot E$, red line) magnitudes. The channel position corresponds to the black line on the inset picture of the pitchfork channel, with 0 μm in the inlet channel and 75 μm on the shallow facet. These data are derived from a Laplace simulation of the wet-etch geometry of the pitchfork channel. The scales are normalized to 1. The relative values of $\nabla E \cdot E$ at the two circles are 1.29 (red circle) and 0.72 (green circle). $\nabla E \cdot E$ at the facet on the black line of the inset is normalized to 1.00.

However, an advantage of the pitchfork design is that samples can be concentrated continuously, minimizing the importance of such dispersion. In such a device, downstream diagnostics could be run continuously, collecting signal as concentrated sample flows by.

Samples of labeled *B. subtilis*, 200-nm particles, and a mixture of both were introduced at the inlet reservoir of the pitchfork channel geometry. The applied potential was systematically chosen in an effort to determine the inhibition threshold field strength for *B. subtilis*. Figure 6a shows *B. subtilis* flowing unhindered down the three exit channels in experiments at applied fields up to 10 V/mm. Figure 6b shows that at and above an applied field of 30 V/mm the flow of *B. subtilis* was restricted to the central channel as a result of DEP deflection by the insulating ridges. The observed behavior indicates an inhibition threshold voltage of 30 V/mm for *B. subtilis* in this device. As the applied electric fields investigated were below the inhibition threshold for the 200-nm polystyrene particles, dielectrophoresis produced by the insulating ridges was negligible and the 200-nm particles flowed uninhibited down each of the three exit channels.

To show that *B. subtilis* could be selectively concentrated and separated from a two-component mixture, *B. subtilis* (6 × 10⁷ cells/mL) and 200-nm particles (4.5 × 10⁸ particles/mL) were mixed and introduced into the device. Upon application of fields up to 30 V/mm, both types of particles passed through the three exit channels. At 30 V/mm, the *B. subtilis* flow was confined to the central channel while the 200-nm particles continued to flow freely through the three outlet channels, demonstrating the feasibility of IDEP as a sample concentrator and fractionation technique. Clearly visible over one of the faceted ridges in Figure 6c is the adhesion of beads to the surface of the channel. This resulted when loading the channel during earlier experimental runs and does not result from electrokinetic or dielectrophoretic effects. Such fouling is caused by sticking of polystyrene particles and limits the number of useful runs for each channel to a few repeated cases.
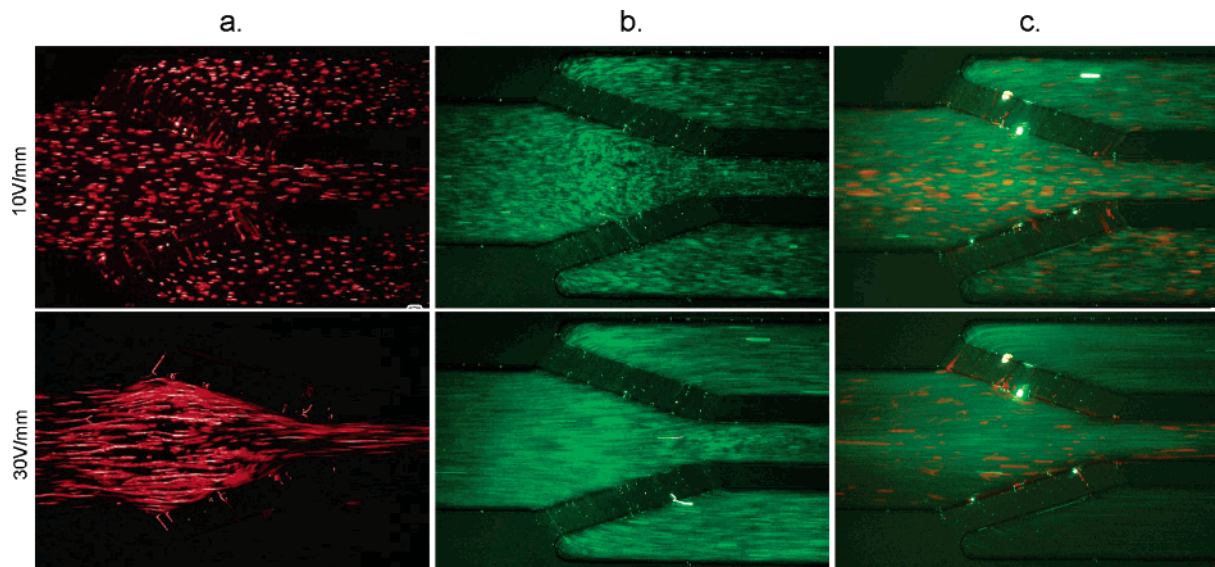
Figure 6. Particle-specific confinement using IDEP. Flow is from left to right. (a) *B. subtilis* (6×10^6 cells/mL) confined by DEP to flow down only the center channel at $E = 30$ V/mm. Note that *B. subtilis* shown here were labeled green (Syto 11) but are falsely colored red for consistency. (b) The 200-nm particles (4.5×10^7 particles/mL) flowing freely through all three outlet channels, (c) Two-component sample of *B. subtilis* (6×10^7 cells/mL) and 200-nm particles (4.5×10^8 particles/mL).

Deviations from ideal channel design result in variations of patterned field gradients along ridge interfaces. In this case, the consequence is imperfect filter/concentrator operation, since the peak value of $\nabla(E \cdot E)$ is not uniform along the interface between deep and shallow sections. In the case of the pitchfork design shown in Figure 5, the peak value of $\nabla(E \cdot E)$ at the red and green circles is 129% and 72% of the value at the intersection of the black line with the facet-deep channel interface. This results in some sporadic leakage of *B. subtilis* into the outer channels at threshold operation. This leakage occurs at the side walls of the ridge structures where there is curvature due to the isotropic etch. Although the rate of leakage is small, it indicates that the present designs could be improved. For example, recent experimental studies of the velocity fields in these channels have led to predictions for which the channel width and depth can be chosen for a deviation in field uniformity at a given location in the channel.[49] Future improvements will employ these design predictions to improve filter/concentrator operation.

The present data are limited to run times for which pressure buildup in the exit port is negligible. For longer runs, buildup of pressure head may cause unwanted effects from pressure effects on the behavior of the ridged concentrator. For example, back pressure can cause a change in the field distribution for faceted prism design, as was demonstrated by Skulan and co-workers.[49] Consequently, the spatially nonuniform field distribution will likely cause particle leakage along the interface of faceted ridges. Back pressure will also introduce a pressure force on particles as they travel downstream, working largely against electrokinetic forces—this should result in lower threshold fields than normally observed. Pressure flow might also cause boundary layer effects, where particles can leak near walls. If required, several methods could be used to minimize the influence of a buildup of pressure. For example, larger inlet and outlet reservoirs would reduce the buildup of pressure head differences as a function of time. In addition, channel coatings could be applied to reduce electro-osmotic flow for a given applied field strength.

A number of examples have been published in recent years demonstrating the use of insulating structures incorporated into microchannels. For instance, numerous papers have been published[36,37,42] for which dielectrophoresis is demonstrated in an array of posts. These posts are constructed using a single etch, such that posts extend from the channel floor to the cover and are, therefore, inherently easier to construct than the present two-level devices. For the post arrays, dielectrophoresis results from the squeezing of fields between rows of posts. In one past demonstration, *Escherichia coli* is trapped at 200 V/mm while 200-nm beads flow freely through the array of posts. Therefore, the applied field magnitudes needed to affect cells by dielectrophoresis are generally larger than for the present study. Nevertheless, such a comparison is not trivial. For example, particles that are not trapped by the first row of posts can have their motion modified, which, in turn, impacts whether they trap at subsequent post rows. Moreover, particles that are trapped can then impact the trapping dynamics of particles that arrive at later times—an effect that can be substantial for comparatively large concentrations.

The function of post arrays is to trap particles at an array of locations within the channel. This inherently disperses filtered samples at many locations in a channel. Detection can then be achieved through techniques such as laser-induced fluorescence within an array, or alternatively, the voltage can be dropped, releasing the particles for downstream diagnostics. This requires synchronization of the sample with downstream analytical instruments and introduces the need to deal with sample dispersion from a sample that is distributed in an array. The use of ridges oriented perpendicular to the direction of flow (Figure 2) also implements a trap-and-release operation with detection along a line, or similarly, sample can be released for downstream analytical detection. The amount of concentration can be increased by increasing the trapping time. The use of angled interfaces enables particle deflection, in which particles are selectively concentrated. This enables continuous operation, for which the concentration channel is monitored continuously by downstream analytical

methods. The degree of concentration is determined by the splitter geometry, with the amount of concentration increasing as the width of the faceted prism channels increases with respect to the width of the central concentration channel. Continuous concentration simplifies the synchronization of downstream analytical instruments with the dielectrophoretic concentrator but replaces it with the need to match flow rates downstream.

CONCLUSIONS

We have presented the first demonstration of particle filtration and concentration using dielectrophresis with insulating ridges. Based on the faceted prism methodology, these can be used to trap, deflect, and concentrate particles selectively. Allowing both batch and continuous processing, these faceted geometries promise to facilitate the rational design of particle and cell manipulation devices for applications in sample preparation, analysis, and detection. The devices presented were created using a two-level etch process of an insulating substrate, which produced channels having insulator-based ridges. Conceptually, the ridge design of Figure 2 can be employed to trap particles selectively in desired locations of a microchannel to support practical device functions. For example, particles can be detected directly at these locations or held in position for chemical reactions (i.e., labeling) or washing steps. Alternatively, particles can be released after a desired period of trapping/concentration for later batch processing. The device shown in Figure 5 demonstrates the potential use of IDEP in a continuous processing mode. This device could be used as is shown here to remove one particle type (*B. subtilis*) from a multicomponent mixture. IDEP also has the ability to be used to deflect, continuously, particles down side channels for further processing.